PLOS One

RESEARCH ARTICLE

Astaxanthin limits atherosclerosis and dysmetabolism in mice by attenuating inflammatory cell recruitment and signaling

Nathaly Anto-Michel[1], Clemens Diwoky[2], Katharina Pfeil[1], Heinrich Mächler[3], Andreas Zirlik[1]*

1 Department of Cardiology, University Heart Center Graz, Medical University of Graz, Graz, Austria,
2 Institute of Molecular Biosciences, University of Graz, Graz, Austria, 3 Department of Cardiac Surgery, University Heart Center Graz, Medical University of Graz, Graz, Austria

* andreas.zirlik@medunigraz.at

Abstract

Introduction

Astaxanthin (ASX) has demonstrated various cardioprotective effects, including reductions in body weight, adipose tissue mass, hypertension, myocardial infarct size, and oxidative stress markers. Despite these findings, the underlying mechanisms remain unclear. This study examines the role of ASX in murine atherosclerosis and metabolic derangements induced by atherogenic diet, aiming to gain a deeper understanding of its biological effects and potential therapeutic applications.

Methods

Ldlr-/- mice were fed a high-fat, high-cholesterol diet (HCD) for 16 weeks, receiving 70 mg/kg ASX or vehicle every other day. A week before the study ended, glucose and insulin tolerance tests were performed. Plaque size in the aorta was analyzed via histology (Oil-red-O and Masson's trichrome). Flow cytometry assessed immune cells from blood, aorta, adipose tissue, and cytokines in plasma. Additional mice underwent intravital microscopy for further investigation.

Results

The overall body weight of animals treated with ASX or vehicle did not differ. ASX-treated mice showed a reduced abundance of peripheral monocytes by 34%, lower numbers of leukocytes in adipose tissue depots, and improved glucose metabolism and insulin sensitivity compared with animals receiving vehicle. White adipose mass decreased while brown adipose and muscle mass increased in mice treated with ASX. Atherosclerotic lesions of Ldlr$^{-/-}$ mice receiving ASX were significantly smaller and contained fewer lipids (3.3 vs 2.6 x 10^5 μm2) and M1 macrophages (0.97 vs

0.42×10^3) but increased collagen, in line with a more stable plaque phenotype. Mechanistic experiments revealed that ASX attenuated leukocyte recruitment ($43\% \pm 1.87$) to the vessel wall in intravital microscopy and dampened inflammatory signaling through Mitogen-activated protein kinases.

Conclusion

ASX treatment reduces experimental atherosclerosis and blunts metabolic syndrome features in mice. This effect is linked to reduced leukocyte recruitment and systemic/local inflammation. The findings support ASX's potential in treating atherosclerosis and metabolic diseases, offering new mechanistic insights and ultimately warrant the rigorous clinical evaluation of such putative effects.

Introduction

Atherosclerosis is a chronic inflammatory disease driven by immune and inflammatory responses at all stages, from onset to complication. Despite advances in cardiovascular treatments, it remains a leading global cause of death [1,2]. Recent research highlights the role of immune cells, opening doors to therapies like antigen-specific immunomodulation and vaccines [3].

Obesity, especially visceral fat from poor lifestyle habits, significantly raises the risk of atherosclerosis and related events such as heart attack and stroke [4]. When combined with hypertension, dyslipidemia, and insulin resistance, it forms metabolic syndrome—a major cardiovascular threat now reaching epidemic levels worldwide [5].

Interestingly, obesity and, more so metabolic syndrome come with a systemic increase in inflammatory markers known to associate with cardiovascular events and outcome [6]. Obese visceral adipose tissue represents a highly active endocrine organ and a major source of such cytokines (pro-inflammatory marker C-reactive protein, tumor necrosis factor α and interleukin-6) and adipokines (resistin, visfatin, adiponectin and leptin), likely promoting deleterious crosstalk between pathologically activated components of the immune system and the vascular endothelium. These phenomena ultimately result in the development of atherosclerotic plaque [7]. In fact, upon onset of obesity [8,9], classically activated macrophages and CD8+ T-cells infiltrate adipose tissue in ways very similar to their infiltration of nascent atherosclerotic plaques, rendering obesity an inflammatory disease with similar properties as atherosclerosis [10].

Astaxanthin (ASX) is a fat-soluble xanthophyll carotenoid synthesized from seaweed, such as Chlamydomona, naked algae, Cynaobacteria or Heamaytococcus pluvalis [11]. The latter presents a higher ASX extraction yield (1.5%−3%) and might be the best biological source of ASX [12]. Therefore, the best product choice is the indoor system employing LED light from Biolife, Austria. Here, the substrates of the freshwater algae are growing; they are reddened, separated, and dried. In the last ten years, ASX presented considerable antioxidant properties. Various preclinical

studies associated ASX exposure with favourable cardiovascular effects, such as reduction of inflammatory biomarkers, markers of oxidative stress and lipid peroxidation, fat accumulation, blood pressure, and infarct size after experimental myocardial infarction [13–16]. Three promising placebo control clinical trials described that supplementation with ASX (from 8 to 20 mg/day) improves LDL, HDL, and triglyceride levels, decreases oxidation of fatty acids, and reduces bio-markers of oxidative stress, such as malondialdehyde and isoprostanes [15,17,18]. In male Swiss albino mice fed a high-fat-high-fructose diet, astaxanthin supplementation (6 mg/kg/day) for 60 days improved insulin sensitivity by enhancing insulin receptor signaling and reducing oxidative stress and inflammation in skeletal muscle and adipose tissue [19]. In a rat model of peritoneal fibrosis, oral administration of astaxanthin attenuated the infiltration of monocyte chemoattractant protein-1 (MCP-1)-positive cells. It suppressed MCP-1 mRNA expression, indicating its potential in preventing fibrosis-related complications [20]. Supplementation with astaxanthin-rich extract for 30 weeks resulted in significant reductions in body weight, serum and liver lipid accumulation, and aortic atherosclerotic lesions. Additionally, ASX improved retinal health and modulated gut microbiota, indicating systemic benefits beyond lipid regulation [21]. It has also been reported that ASX supplementation promoted reverse cholesterol transport (RCT), a process that facilitates the removal of excess cholesterol from macrophages and reduces aortic cholesterol content [22]. These studies highlight that ASX can affect the development of atherosclerosis. However, the exact mechanism of ASX in atherosclerosis development is unknown. Here, we investigate the impact of ASX on experimental atherosclerosis in Ldlr−/− mice (Fig 1).
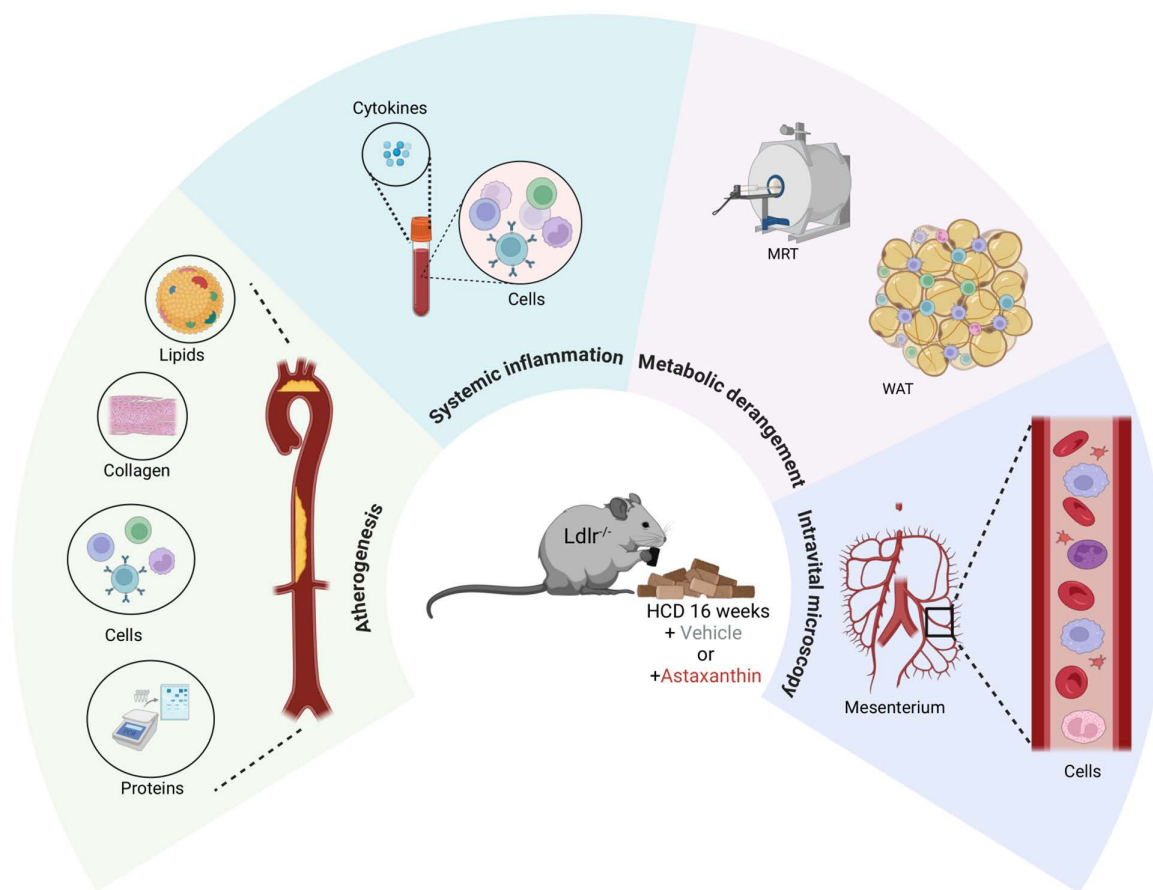

Fig 1. Scheme of the experimental design. Atherogenesis, metabolic parameters, inflammation and molecular pathways with the help of histology, flow cytometry, MRT and intravital microscopy were assessed Ldmlr−/− mice on HCD received ASX or vehicle every second day for 16 weeks.

https://doi.org/10.1371/journal.pone.0334410.g001

Materials and methods

Animals and treatment

Male and female Ldlr knockout mice 8-week-old were used and housed in conventional cages under standard conditions and *ab libitum* access to water and High cholesterol diet (HCD) containing 1.25% cholesterol and 17% cocoa butter (Sniff Spezialdiäten GmbH, D1208). Animals received Astaxanthin (70 mg/kg) or vehicle (sunflower oil) every other day via gavage ($n = 15$ per group). Mice were on HCD and treatment for 16 weeks. At the end of the study animals were harvested and histologically analyzed as described previously [23,24].

The mice were purchased from Jackson Laboratory (B6.129S7-Ldlrtm1Her/J). All mouse experiments were performed in accordance with the Guide for the Care and Use of Laboratory Animals published by the US National Institutes of Health and were performed after securing approval from the Federal Ministry of Education, Science, and Research, Austria. (TVG: 2021-0.009.980)

The method of euthanasia used was Carbon dioxide (CO_2) inhalation, and depending on the experiment, analgesics (ketamine and xylazine) were used to eliminate/alleviate suffering.

Oil Red O staining

Frozen sections were fixed with 10% neutral buffered formalin for 10 min at room temperature. Sections were incubated with propylene glycol for 2 min, then with pre-heated Oil Red O staining solution (American MasterTech, STOROPT) at 60 °C for an additional 8 min. Sections were placed in 85% propylene glycol for 1 min and counterstained with modified Mayer's hematoxylin (American MasterTech, HXMMHLT) for 1 min, rinsed with water, and then mounted with glycerine jelly (Fisher Scientific, NC0301797).

Masson's trichrome staining

Aortic roots were cut into 5-µm sections and stained by Masson's trichrome stain to detect collagen deposits. Instructions were followed as indicated by Sigma Aldrich (HT15).

Adipose tissue arrangement

Body composition was determined using a 7 Tesla (Biospec 70/20, Bruker, Ettlingen, Germany). Anesthesia was induced by placing the mice for 3–4 min in a chamber of 4% isoflurane in O2. During magnetic resonance imaging (MRI), the anesthetic level was maintained by 1.8–2.0% isoflurane in O2 (1 L/min) to keep the respiration rate between 80 and 100 bpm. Mice breathed freely, and animal body temperature was maintained by a water-heated animal bed. Mice were scanned in supine position. A balloon pressure sensor (SA Instruments Inc, NY, USA) was placed on the abdomen for respiratory gating. For adipose tissue segmentation, a T2-weighted respiratory gated 2D fast spin echo sequence was used with the following parameters: TR/TE = 2200/28.8 ms, turbo factor = 13, slice thickness = 500 µm, in-plane resolution = 156 × 156 µm, FOV = 40 × 40 mm, 30 slices. The ingWAT, PVAT, and visWAT were manually segmented in ITK-Snap [25]. For quantitative lipid mapping, a proton density fat fraction measurement was carried out [26] employing a respiratory-gated multi-echo gradient echo sequence with the parameters: TR = 700 ms, alpha = 20°, 8 monopolar echoes with TE = 1.6/2.8/3.9/5/6.2/7.3/8.4/9.6 ms, slice thickness = 500 µm, in-plane resolution = 219 × 219 µm, FOV = 35 × 35 mm, 55 slices. Proton density fat fraction was fitted from the multi-echo data using a variational approach, including B0-field correction [27].

Intraperitoneal glucose tolerance testing (GTT) and insulin tolerance testing (ITT)

Glucose and insulin tolerance testing was performed after 16 weeks of HCD as described previously [28]. In brief, mice were fasted 8 hours before the test. For GTT, mice received an intraperitoneal glucose injection (1g/kg body weight). For ITT, mice were injected with human insulin intraperitoneally (0.5 U/kg, Actrapid Insulin, Novo Nordisk, Denmark). Blood

samples were collected at 0, 15, 30, 45, 60, 90, and 120 minutes after the glucose or insulin administration, and plasma glucose concentration was measured with an AccuChek GO (Roche Diagnostics, Switzerland). As indicated, area-under-the-curve analysis (glucose concentration in mg/dl over time in minutes) was calculated per animal.

Isolation of stromal vascular fraction (SVF)

Murine visceral fat pads were minced and digested with collagenase I (0.5 mg/ml) for 30 minutes at 37°C. Digested tissue was filtered through a cell strainer (100 µm). The adipocyte fraction was collected from the floating top layer, and the pellet (SVF) was collected for further FACS analysis.

Flow cytometry

FACS analysis was performed as described previously [29]. In brief, cells were washed in PBS and stained with viability dye for 30 min on ice. Cells were washed with FACS buffer (PBS$^{-/-}$/1% FCS) and incubated with the indicated antibodies (all from Biolegend, 1:200) before quantification on a flow cytometer (CytoFlex Beckman). Leukocyte populations were identified as CD45 + viability dye- cells and upon cell surface expression of the indicated antigens (S1 Table): T-helper cells (CD3+ CD4+ CD8−), cytotoxic T cells (CD3+ CD4− CD8+), T-regulatory cells (CD4+ CD25+ FoxP3+), B cells (CD19+) or dendritic cells (F4/80− CD11c+). Adipose tissue macrophages were identified as CD45+ CD11b+ CD3− CD19− F4/80+ or M1 macrophages + CD11c+.

Plasma sample analysis

Plasma levels of FFAs were measured by a commercial enzymatic method using 3-methyl-N-ethyl-N- (β-hydroxyethyl)-aniline (MEHA) as a violet color agent according to the manufacturer's protocols (LabAssay NEFA, USA). An enzymatic-colorimetric test determined triglyceride and total cholesterol levels (DiaSys, Germany).

Inflammatory markers in plasma

Levels of Interleukin-6 (IL-6), Interleukin-10 (IL-10), Monocyte Chemoattractant Protein-1 (MCP-1), Interferon-γ (IFN-γ), Tumor Necrosis Factor (TNF), and Interleukin-12p70 (IL-12p70) were determined by bead array (BD™ Cytometric Bead Array (CBA)).

Gene expression

Freshly collected abdominal aortas were stored in RNAlater (Qiagen, Germany). RNA was extracted by TrizolLS (Invitrogen, USA) and glycogen as a co-precipitator (Roche, Switzerland). Homogenization was performed using a rotor-stator dispergator (IKA, Germany). 1 µg of total RNA was transcribed into cDNA using the iScript Synthesis Kit (Bio-Rad, Germany). Subsequent quantitative PCR was performed using the SYBR green Master Mix (ThermoFischer, USA) detection format. α-Actin and GAPDH served as control as indicated (S2 Table).

Intravital microscopy

Intra-vital microscopy was performed as previously described [30]. In brief, mice on WD and ASX or vehicle per 10 days before surgery received intraperitoneal injections of Murine TNFα, 200ng (R&D systems), and surgery started four h later. Briefly, mice were anesthetized by intraperitoneal injection of ketamine hydrochloride (100 mg/kg; Essex, USA) and xylazin (5 mg/kg; Bayer, Germany). The mesentery was exteriorized and placed under an upright intravital microscope (AxioVision, Carl Zeiss, Germany). Videos of rolling and adhering in mesenteric venules were taken after retro-orbital injection of rhodamine (0,025 mg/kg; ~60 µL of 1 mg/mL). Rolling leukocyte flux was defined as the number of leukocytes moving at a velocity less than erythrocytes. Adherent leukocytes were defined as cells that remained stationary for at least 30 s.

Western blot

Aorta tissue samples were lysed, separated by SDS-PAGE under reducing conditions, blotted to polyvinylidene difluoride membranes, and stained against the indicated antibodies, total p38 MAPK (Cell Signaling, 9212S, 1:1000), phosphorylated p38 MAPK (Cell Signaling, 9211S, 1:1000), followed by a visualization with Clarity Western ECL Substrate (Biorad, 170–5061). For quantification of protein expression, the density of the specific targets was normalized to GAPDH (Clone 14C10, Cell Signaling 2118S, 1:1000) and expressed as the ratio of phosphorylated protein/total protein.

Statistical analysis

Data are presented as mean $\pm$ standard error of the mean (SEM), and p-values less than 0.05 were considered statistically significant. Statistical testing employed a 2-sided, unpaired Student's T-test between the groups for normal distributed variables and a Mann-Whitney Test for non-normal distributed variables. Differences across three or more groups were tested with ANOVA with Turkey's multiple-comparison test or multiple T-tests with Holm-Sidak corrections for multiple comparisons. For time courses of two groups, repeated measures, 2-way ANOVA was tested.

Results

Astaxanthin treatment results in smaller atherosclerotic lesions showing features associated with plaque stability

To investigate the role of ASX in murine atherogenesis, Ldlr$^{-/-}$ mice consumed a high cholesterol diet (HCD) supplemented with ASX or vehicle (sunflower oil) for 16 weeks, starting at 8 weeks of age. Animals treated with ASX (5.65×10^5 $\mu m^2 \pm 0.36$) exhibited significantly smaller atherosclerotic plaque areas at 16 weeks than animals receiving vehicle (7.29×10^5 $\mu m^2 \pm 0.36$, N = 18, P = 0.01). Histologic analysis of plaque composition revealed that atherosclerotic lesions from ASX-treated animals had reduced lipid content as measured by Oil-red—O ($3.3 \times 10^5/\mu m^2 \pm 0.10$ in vehicle vs. $2.6 \times 10^5/\mu m^2 \pm 0.14$ in ASX, N = 18, P = 0.004, Fig 2A and 2B). In contrast, while total leukocyte numbers did not differ between the groups (Fig 2E), overall macrophage infiltration increased in the plaques of ASX-treated mice; however, the M-1 subtype, known to be pro-atherogenic, was significantly less abundant (Fig 2F and 2G) in the ASX group ($0.97 \times 10^3 \pm 0.18$ in vehicle vs 0.42 x$10^3 \pm 0.06$ in ASX, N = 18, P = 0.03). Other leukocyte subpopulations, such as granulocytes, T helper, and T cytotoxic cells, showed no changes (S1 Fig A-C). Given that M1 macrophages release pro-inflammatory cytokines during inflammation, we examined the gene expression of IL-6, TNFα, and IL-1β in the aorta. Consistent with the observed reduction in inflammatory M1-polarized macrophages, the overall inflammatory burden of plaques from ASX-treated animals was significantly lower, as indicated by very low expression levels of IL-6, TNFα, and IL-1β (Fig 2I). Further morphological analysis of the roots using Mason's trichrome staining also revealed increased collagen content ($26.14\% \pm 1.54$) compared to the control group ($45.34\% \pm 1.37$, N = 18, P = 0.001) (Fig 2C and 2D). Overall, this extensive phenotypic analysis suggests that the smaller atherosclerotic lesions seen in ASX-treated animals are less inflamed due to a decrease in the pro-inflammatory M1 phenotype of macrophages, which correlates with reduced production of pro-inflammatory cytokines and indicates signs associated with increased plaque stability [31–33].

Animals treated with Astaxanthin show reduced numbers of inflammatory monocytes and attenuated levels of pro-inflammatory cytokines

Flow cytometry analysis of the blood showed that the fraction of circulating monocytes analyzed by expression of CD45$^+$/CD11b$^+$/CD115$^+$/Ly6G$^-$ was reduced from $2.9 \times 10^9/L \pm 0.35$ in the vehicle group to $1.9 \times 10^9/L \pm 0.19$ in the ASX group (N = 18, P = 0.02, Fig 3A-3C). At the same time, other myeloid subpopulations were unaffected by ASX treatment (S2 Fig A, B). Notably, the numbers of inflammatory monocytes expressing high levels of Ly6C were reduced by 36% (Fig 3B), a cell fraction known to propagate atherosclerosis and its sequelae [34,35].
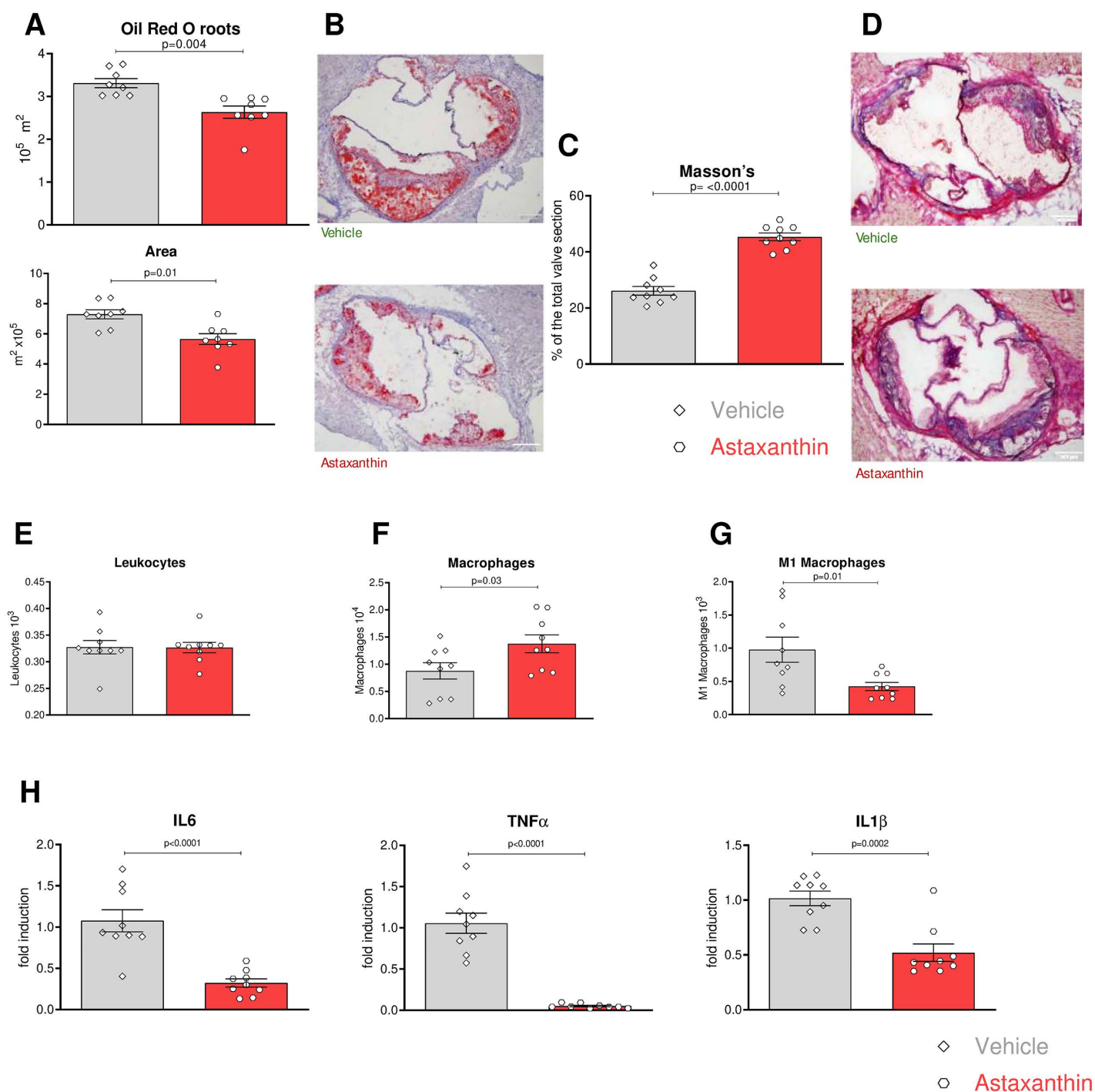
Fig 2. Atheroprotective effect of Astaxanthin. (A) Quantification of lipid content and atherosclerotic plaque area. **(B)** Representative picture of the aortic root sections stained with Oil-Red-O (ORO) and hematoxylin. **(C)** Sections of the aortic root were analyzed for collagen content; positive staining is displayed as mean±SEM duplicates (N = 9 per group, 5 males, 4 females). **(D)** Masson's Trichrome staining. **(E, G)** Total Leukocytes, macrophages and M1 pro-inflammatory population identified in the digested aorta (n = 9 per group, 5 males, 4 females) by flow cytometry. **(H)** Gene expression of IL6, TNFα, and IL1β on qPCR from whole abdominal aorta. An unpaired T-test assessed (A, C, E-G) Significance.
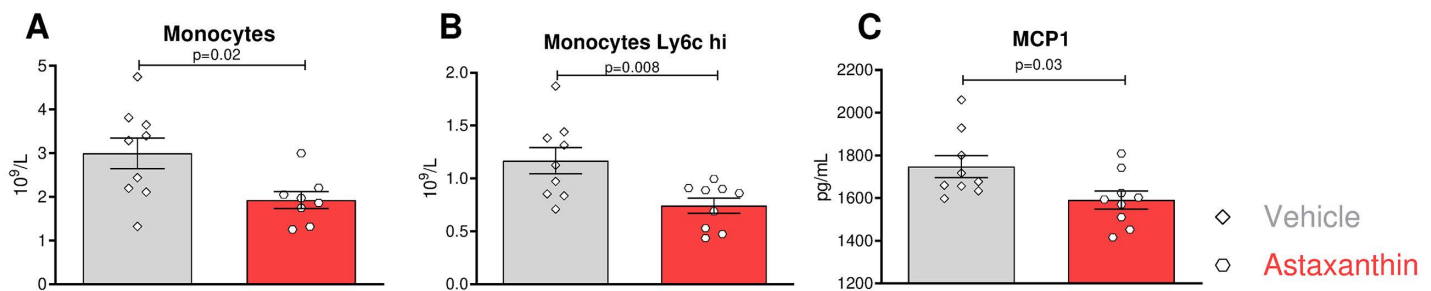
Fig 3. Astaxanthin's effects on circulating monocytes. (A) Monocyte subsets were identified using flow cytometry in peripheral blood following the lysis of erythrocytes. **(B)** Surface expression of Ly6c on peripheral monocytes was analyzed by flow cytometry. **(C)** Plasma levels of MCP1 were measured with a CBA kit. **(A-C)** Significance was evaluated with an unpaired T-test. N = 9/8 (5 males, 4 females vs 4 males and 4 females).

The number of circulating B and T cells and their different subsets did not show significant differences between the control and treated groups (S2 Fig D-H). However, analysis of inflammatory cytokines in the plasma by cytokine bead array revealed significantly decreased levels of pro-inflammatory MCP1 cytokine in the ASX group (1591pg/mL ± 42.20) compared to the control group (1748pg/mL ± 51.44, N = 18, P = 0.03, Fig 3C), whereas concentrations of TNFα, IFNγ, IL10, IL-6, and IL-12 cytokines did not differ between the two groups (S2 Fig I-M). These data strongly suggest that ASX also enfolds less pro-inflammatory immune profile in the periphery.

Astaxanthin limits inflammatory cell recruitment to the vessel wall and reduces MAP-kinase activation

To explore mechanisms explaining the reduced content of inflammatory macrophages in the atherosclerotic plaques of ASX-treated animals, we tested whether ASX may affect the rolling and adhesion of inflammatory cells, crucial steps in the recruitment of inflammatory cells to sites of inflammation. Therefore, mice were subjected to intravital microscopy in the presence of Astaxanthin or vehicle 1 day before challenging them with systemic injection of TNFα for four hrs. Fewer leukocytes rolled (94.5 cells ± 10.68 vs 68.64 cells ± 7.95, N = 20, P = 0.05) and adhered (10.10 ± 1.72 cells vs 4.4 cells ± 1.01, N = 20; P = 0.005) to the peritoneal vessels in the group treated with Astaxanthin (Fig 4A-4C). These results tempted us to verify potential outside signaling events promoted by ASX. Accordingly, some abdominal aortas of the treated Ldlr$^{-/-}$ mice were used for protein isolation, and phosphorylation of Mitogen-activated protein kinase (MAP) p38 in Western blotting was determined. We observed an enhanced phosphorylation of MAP-kinase p38 in the control group, indicating that known leukocyte activation and adhesion result of MAPK pathway activation, is blocked by Astaxanthin (Fig 4C). These results indicate that Astaxanthin reduces leukocyte adhesion and accumulation via a reduction in the p38 MAPK activation.

Application of Astaxanthin ameliorates key features of metabolic derangements induced by atherogenic diet in mice

A diet high in cholesterol and lipids not only induces atherosclerosis but also contributes to the characteristics of metabolic derangements [36,37]. To determine whether ASX impacts the metabolism of Ldlr$^{-/-}$ mice on a high-cholesterol diet (HCD), animals treated with ASX or vehicle control were evaluated for signs of metabolic imbalances. Although body weights throughout the feeding period and the weights of other organs at the conclusion of the study did not vary significantly between the two groups (S3C Fig). To evaluate body fat distribution, mice underwent MRI screening (Fig 5A, 5B), and the volumes of inguinal, visceral, and perivascular adipose tissue were measured. Animals given Astaxanthin demonstrated a significant and consistent decrease in total volume and neutral lipid mass (signal from fatty acid chains) across the three different adipose tissue depots (Fig 5C-5E), indicating that Astaxanthin helps prevent the accumulation of adipose tissue.
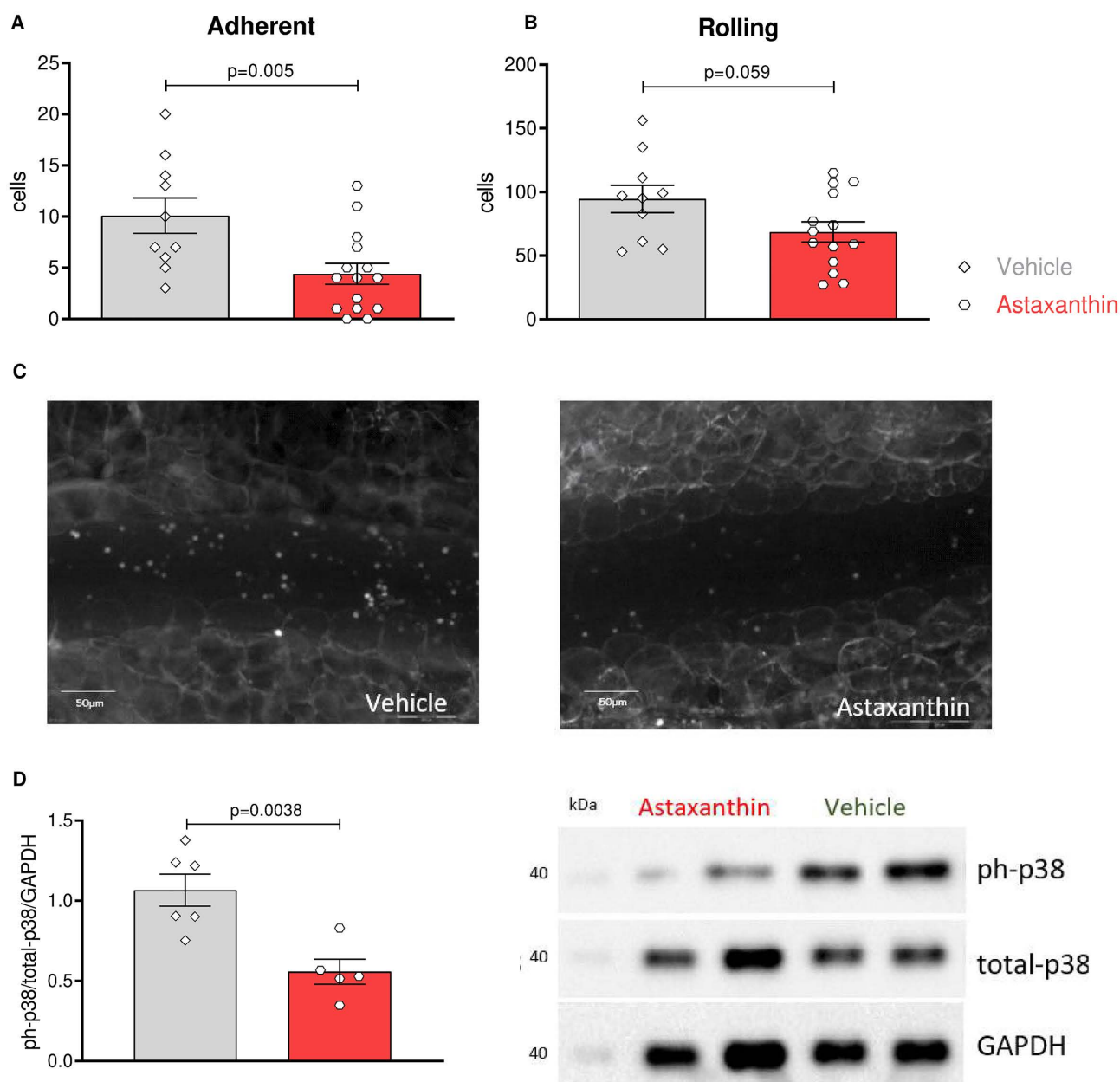
Fig 4. Treatment with Astaxanthin inhibits leukocyte infiltration and MAP kinase activation. Leukocyte recruitment was observed via intravital microscopy following 4 hours of TNFα stimulation. **(A)** Quantification of adherent and **(B)** rolling leukocytes was performed. Error bars represent mean ± SEM. Statistical significance was determined using an unpaired T-test between the indicated groups. N = 10/15. **(C)** Representative images of intravital microscopy. **(D)** Protein was isolated from the whole aorta, and both total and phosphorylated p38 were visualized by western blot; the ratio of phosphorylated fractions was calculated and normalized to the housekeeping GAPDH. Values were expressed as relative arbitrary units (AU) normalized to the signal from the animals in the control group receiving only the vehicle. N = 6 per group (3 males and 3 females).

A hallmark of adipose tissue inflammation is the infiltration of leukocytes [38]. Therefore, we quantified the number of leukocytes in visceral adipose tissue. Compared to the control group, the group treated with ASX showed a lower number of macrophages (0.77% of viable leukocytes ± 0.09 vs 0.47% of viable leukocytes ± 0.08, N = 18, P = 0.03) and some
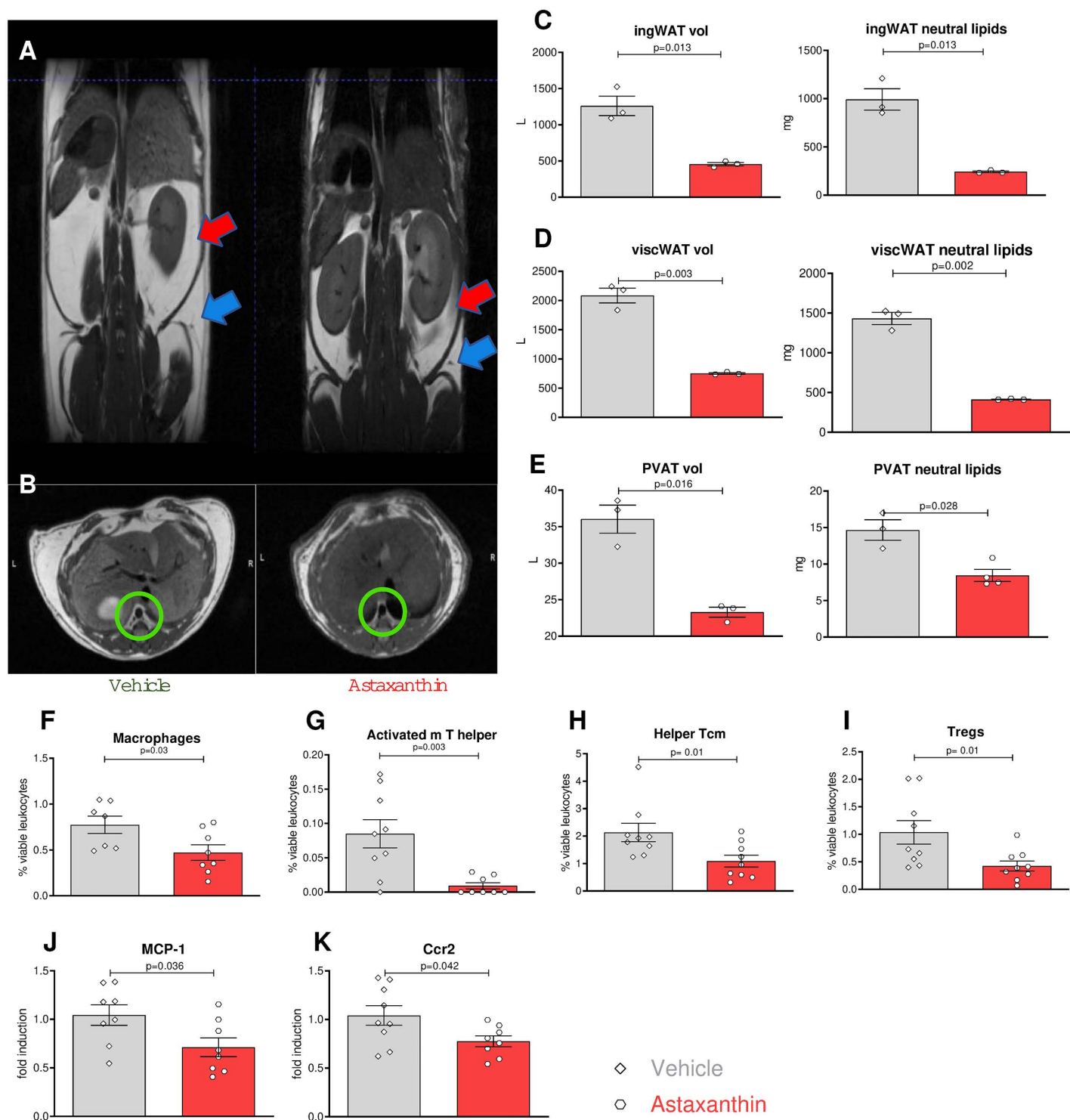
Fig 5. Astaxanthin reduces adipose tissue dysfunction. (A) Visceral adipose tissue (red arrow), subcutaneous adipose tissue (blue arrows), and **(B)** perivascular adipose tissue (green circle) were imaged using MRI (white signal). Fat pad volume and neutral lipids in **(C)** inguinal, **(D)** visceral, and **(E)** perivascular compartments. **(F-I)** Leukocyte subsets were identified through flow cytometry of visceral adipose tissue cells after the tissue was digested. Transcripts of MCP-1**(J)** and CCR2 **(K)** measured by qPCR. Error bars represent mean±SEM. Statistical significance was assessed using an unpaired T-test between the indicated groups. N = 9/9 per group (5 males and 4 females).

subtypes of T cells (Fig 5F-5I). Furthermore, MCP-1 and CCR2 mediate monocyte recruitment to white adipose tissue, promoting inflammation and insulin resistance in obesity. Hence their transcript expressions were determined in adipose tissue, and we found a reduction of both in the astaxanthin group (Fig 5J and 5K).

Unexpectedly, muscle and brown adipose tissue (BAT) weights were notably greater in the Astaxanthin-treated group (Fig 6A, 6C). Additionally, the ASX group showed a marked reduction in white adipose tissue (WAT) (Fig 6B). One consequence of obesity is the development of insulin resistance and dyslipidemia. However, no differences in plasmatic lipid levels were found (S3 Fig G-I) between the two groups. In line with the reduction of WAT, the group receiving Astaxanthin presented with significantly lower fasting glucose levels (Fig 6D). In accord, the Astaxanthin group showed lower glucose concentrations in blood during an intraperitoneal glucose and insulin tolerance test (Fig 6E-6H). Collectively, our findings identify a protective effect of Astaxanthin against metabolic derangements induced by atherogenic diet.

Discussion

In this study, we report that astaxanthin reduces atherosclerotic plaque formation and alleviates symptoms characteristic of metabolic syndrome. Our data challenge the traditional view of studying diseases in isolation by presenting results from an atherosclerotic model combined with metabolic data. Hypercholesterolemia has been shown to induce impaired glucose tolerance and insulin sensitivity in Ldlr$^{-/-}$ mice previously due to lower insulin secretion in pancreatic islets, and the insulin secretion defect extended to other fuel secretagogues like l-leucine and 2-ketoisocaproic acid. Cholesterol depletion using methyl-beta-cyclodextrin restored insulin secretion, indicating that the secretion defects were caused by elevated cholesterol [39].

An area of current research is the use of anti-inflammatory agents to battle atherosclerosis and metabolic diseases [40–45]. We previously identified several key inflammatory signal intermediates, such as CD40L, Tumor necrosis factor receptor-associated factors (TRAFs), and danger signaling receptors, as potential targets to regulate the
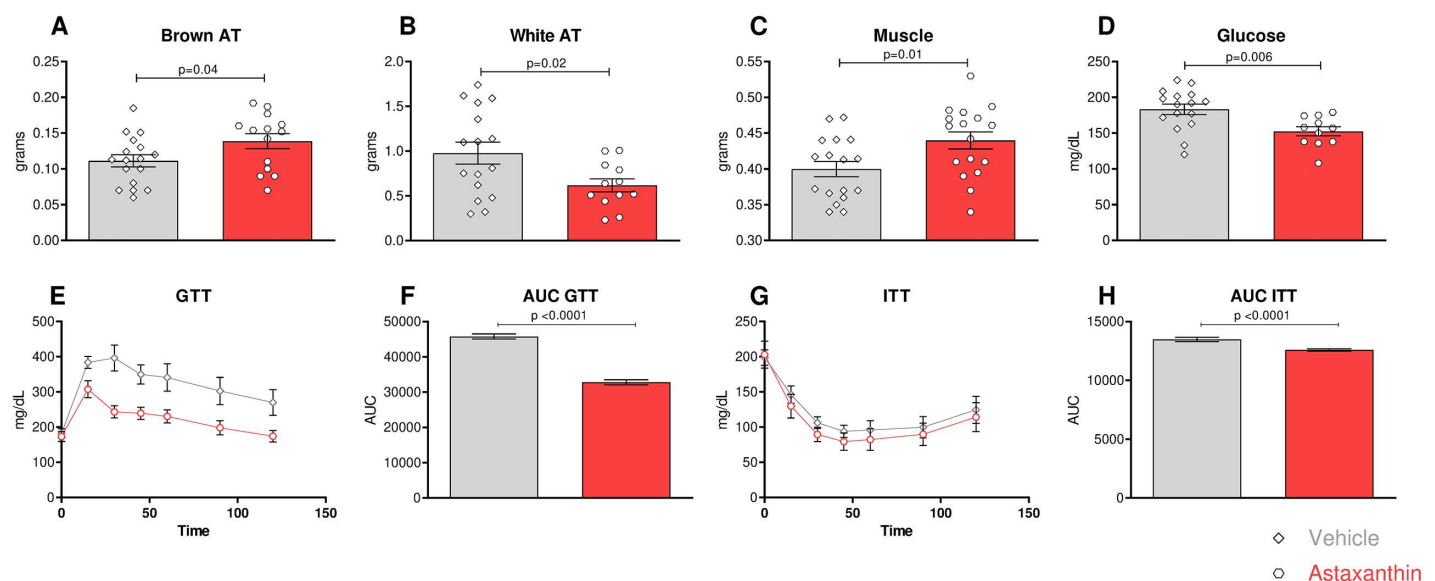

Fig 6. Astaxanthin regulates glucose utilization and insulin sensitivity. (A-C) Weight of brown adipose tissue, white adipose tissue, and muscle after 16 weeks of diet and treatment. **(D)** Glucose levels in fasting animals. **(E)** Glucose tolerance testing (GTT), and (G) insulin tolerance testing (ITT). Injections were based on the total body lean tissue weight. **(F, H)** Area under the curve for glucose or insulin tolerance. Error bars represent mean ± SEM. Statistical significance was assessed using an unpaired t-test between indicated groups (A-D) and repeated two-way ANOVA **(E, G)**. N = 16/16 (9 males and 7 females).

https://doi.org/10.1371/journal.pone.0334410.g006

inflammatory balance in this context [23,28,30,33,43,46–49]. It has been shown that Astaxanthin can inhibit specific pro-inflammatory signals in neurological, gastrointestinal, hepatic, and renal diseases [50]. Our data support anti-inflammatory treatment with Astaxanthin, revealing that ASX attenuates the inflammatory response in atherogenesis. While an atherogenic diet is not sufficient in promoting the onset of genuine diet-induced obesity as a model of what we call the metabolic syndrome in humans, it does induce significant metabolic changes, as seen in the glucose- and insulin-tolerance testing we performed. Interestingly, Astaxanthin also blunted those metabolic derangements caused by the atherogenic diet.

In the present study, Astaxanthin not only reduced the development of atherosclerotic plaques in terms of size but also altered their histological characteristics towards features associated with more stability in humans. These findings are consistent with three studies in ApoE knockout mice using natural astaxanthin, Calanus oil (containing astaxanthin and astaxanthin esters), or CX-085, a synthetic drug of the naturally occurring xanthophyll carotenoid astaxanthin, although the postulated mechanisms differ, Ryu et al. and Eilertsen et al. used animal models but did not identify a clear mechanism explaining how astaxanthin influences the development of atherosclerotic plaque. In contrast, Zhang et al. attribute the effect to the CircTPP2/miR-3073b-5p/ABCA1 pathway. However, this mechanism has only been described in macrophages, limiting its generalizability to other cell types [51–53]. Inflammatory processes are orchestrated by a variety of immune cells, among them differentially activated M1 and M2 macrophages [54,55]. Plaques in the astaxanthin group showed a marked reduction in M1 macrophages, known to propagate proatherogenic inflammation. Intimal M1 macrophages are important contributors to atherogenesis; their accumulation progresses during plaque growth and is associated with thrombotic complications [56,57]. The main processes regulating the macrophage content in plaques are adhesion and migration. To better understand the mechanism by which Astaxanthin modulates macrophage content, we tested whether Astaxanthin affects one of these steps with the aid of intravital microscopy. By stimulating mice with TNFα, the endothelium is expected to be activated. Through the interaction of ICAM-1 and VCAM-1, the adhesion of inflammatory cells to the endothelial cell surface is mediated. We identified that a single dose of Astaxanthin before stimulus can significantly reduce inflammatory cell adhesion to the endothelium in mesentery veins *in vivo*. Some studies have reported that the blockade of the MAPK signaling pathway is often related to this inflammatory process [58,59]. Indeed, we could show that p38 phosphorylation is reduced in atherosclerotic aortas from mice treated with astaxanthin.

Several pro-inflammatory cytokines have been found to play a key role in the development of atherosclerosis, for example, TNFα produced by CD4+T cells and myeloid cells, IL6 that depending on the disease stage, can be either pathogenic or protective, and IL1β produced by myeloid cells, responsible for vascular wall inflammation, due to the upregulation of adhesion molecules by endothelial cells as well macrophage activation [60–64]. Equally, these cytokines have been linked to the onset and progression of adipose tissue inflammation and metabolic syndrome [65–67]. Our experimental data support the idea that astaxanthin is anti-inflammatory, demonstrating inhibition of several of these pro-inflammatory cytokines in our hands, another potential mechanism likely contributing to the effects observed on atherosclerosis and associated metabolic derangements.

Adipose tissue inflammation, with an accumulation of leukocytes and the expression of inflammatory intermediaries that preserve the inflammatory response [68], is a hallmark of obesity. Adipose tissue inflammation results in tissue remodeling and insulin resistance [69]. As anticipated, Astaxanthin alleviated the inflammation of obese visceral adipose tissue, improved metabolism, protected against obesity, and reduced ectopic lipid deposition, possibly by decreasing the number of inflammatory monocytes in the periphery. This, in turn, limited adipose tissue inflammation by reducing the infiltration of macrophages and activated T cells. This decrease in adipose tissue inflammation was not entirely unexpected. Several anti-inflammatory compounds have demonstrated a reduction in pro-inflammatory cytokines, a decrease in macrophage infiltration, and a suppression of adipose tissue inflammation [70].

Other organs, such as the liver, skeletal muscle, brown adipose tissue, and the brain, also contribute to metabolic dysfunction. Improvements in adipose tissue inflammation are usually paired with improvements in other organ functions

that influence insulin sensitivity [71]. It has been observed that an increase in brown adipose tissue and muscle positively affects glucose and insulin metabolism and body mass [72,73]. Although the precise mechanism remains unclear, the metabolic benefits related to glucose utilization and insulin sensitivity in the group receiving Astaxanthin have been linked to higher ratios of brown adipose tissue and skeletal muscle, both of which are crucial for improved glucose homeostasis.

In conclusion, we present the finding that Astaxanthin limits atherogenesis and improves metabolism in mice. The most likely underlying mechanisms include attenuated macrophage recruitment to the vascular wall and adipose compartment, reduced inflammatory signaling and cytokine production, and tipping body composition to increased brown adipose tissue and muscle. Our data corroborate the notion that Astaxanthin is a promising pharmacological tool for cardiovascular pathologies. Given the effects observed, the economic attractiveness of Astaxanthin formulations, and the potential broad impact on health and socioeconomics, this hypothesis should be tested rigorously in well-controlled large clinical collectives.

Supporting information

S1 Fig. Granulocytes and T cells found in adipose tissue are unaffected by astaxanthin. Eight-week-old male Ldlr$^{-/-}$ mice were fed a high-cholesterol diet for 16 weeks. Frequencies of (A) granulocytes, (B) helper T cells, and (C) cytotoxic T cells in the stromal vascular fraction isolated from white adipose tissue were quantified using flow cytometry. Leukocyte subpopulations were identified as follows: Granulocytes (CD11b+, GR-1+, CD115−), helper T cells (CD3+, CD4+, CD8−), and cytotoxic T cells (CD3+, CD4−, CD8+), expressed as a percentage of all live CD45+ leukocytes. Statistical significance was assessed using a two-sided, unpaired t-test (A-C). n = 6 mice per group (3 male and 3 female). (TIF)

S2 Fig. The myeloid and lymphocytic subsets in the blood, as well as the plasmatic levels of cytokines, were not altered by Astaxanthin. Male Ldlr$^{-/-}$ mice were fed a high-cholesterol diet for 16 weeks, starting at an age of 8 weeks. Absolute numbers of (A) peripheral granulocytes (CD11b+Gr1+), (B) dendritic cells (CD11b+CD11c+), (C) natural killer cells (CD11b-NK1.1+), (D) B cells type a (CD19+CD5+), (E) B cells type b (CD19+B220+CD5-), (F) T cells (CD19-CD3+), (G) helper T cells (CD3+CD4+CD8-) in the blood were analyzed. Plasma levels of pro-inflammatory cytokines (H) interleukin 6, (I) tumor necrosis factor alpha, and (J) interferon gamma were measured. Levels of anti-inflammatory cytokines (K) interleukin 10 and (L) interleukin 12 were also assessed. Statistical significance was evaluated using a 2-sided, unpaired t-test (A-M). n = 9 (5 male and 4 female) mice per group. Data are presented as mean ± SEM. (TIF)

S3 Fig. Astaxanthin treatment does not affect whole body weight during the feeding period neither the weight of different organs nor plasma lipids. Ldlr$^{-/-}$ mice were fed for 16 weeks with a high-cholesterol diet and divided into two groups, treated with either vehicle or Astaxanthin. (A) Absolute body weight after feeding. (B) Body weight during the feeding period. (C) Weight of the heart, (D) liver, (E) kidney, and (F) spleen. (G) Cholesterol, (H) triglycerides and (I) Non-esterified fatty acids levels in plasma. Statistical significance was assessed using a two-way (repeated-measures) ANOVA (B) and an unpaired, two-sided T-test (A, C-F). n = 16 (9 male and 7 female) mice per group. Data are presented as mean ± SEM. (TIF)

S1 Table. List of antibodies used for flow cytometry (FACS) analysis. This table details all antibodies used for flow cytometry experiments, including antigen targets, fluorochrome conjugates and clones. Antibodies were titrated for optimal signal-to-noise ratio prior to use. All staining was performed according to the manufacturer's recommendations, and appropriate isotype and fluorescence-minus-one (FMO) controls were included for gating. (PDF)

S2 Table. List of primers used in this study. This table summarizes all primers used for qRT-PCR. The table includes primer abbreviation, protein names and sequences (5′→3′).
(PDF)

S1 Data. Raw gel images. (A) Total p38 MAPK. (B) Phospho-p38 MAPK (p-p38). (C) GAPDH (loading control). Uncropped and unprocessed gel images corresponding to the Western blot data shown in the main manuscript. Each panel represents the raw data used for quantification and analysis in the corresponding figure of the main text.
(PDF)

S2 Data. Minimal data set. Collection of relevant experimental data: (1) body weight over weeks, (2) intravital data, (3) lab blood count, (4) intraperitoneal glucose tolerance testing, (5) insulin tolerance testing, (6–9) FACS results, (10) Oil-red-O staining, (11) Masson's trichrome staining, (12) cholesterol, (13) triglycerides, (14) NEFA measurements, (15) qPCR data, (16) inflammatory marker levels, (17) magnetic resonance imaging, (18) Western blot quantification.
(XLSX)

Author contributions

Conceptualization: Nathaly Anto-Michel, Heinrich Mächler, Andreas Zirlik.

Data curation: Katharina Pfeil.

Formal analysis: Nathaly Anto-Michel, Clemens Diwoky.

Investigation: Nathaly Anto-Michel, Clemens Diwoky.

Methodology: Nathaly Anto-Michel, Clemens Diwoky.

Supervision: Heinrich Mächler, Andreas Zirlik.

Validation: Nathaly Anto-Michel.

Visualization: Nathaly Anto-Michel.

Writing – original draft: Nathaly Anto-Michel.

Writing – review & editing: Heinrich Mächler, Andreas Zirlik.

References

1. Kobiyama K, Ley K. Atherosclerosis: a chronic inflammatory disease with an autoimmune component. Circ Res. 2018;123(10):1118–20.

2. Tabares-Guevara JH, Villa-Pulgarin JA, Hernandez JC. Atherosclerosis: immunopathogenesis and strategies for immunotherapy. Immunotherapy. 2021;13(14):1231–44. https://doi.org/10.2217/imt-2021-0009 PMID: 34382409

3. Wolf D, Zirlik A, Ley K. Beyond vascular inflammation–recent advances in understanding atherosclerosis. Cell Mol Life Sci. 2015;72(20):3853–69. https://doi.org/10.1007/s00018-015-1971-6 PMID: 26100516

4. Powell-Wiley TM, Poirier P, Burke LE, Després J-P, Gordon-Larsen P, Lavie CJ, et al. Obesity and cardiovascular disease: a scientific statement from the american heart association. Circulation. 2021;143(21):e984–1010. https://doi.org/10.1161/CIR.0000000000000973 PMID: 33882682

5. Blüher M. Obesity: global epidemiology and pathogenesis. Nat Rev Endocrinol. 2019;15(5):288–98. https://doi.org/10.1038/s41574-019-0176-8 PMID: 30814686

6. Kawai T, Autieri MV, Scalia R. Adipose tissue inflammation and metabolic dysfunction in obesity. Am J Physiol Cell Physiol. 2021;320(3):C375–91. https://doi.org/10.1152/ajpcell.00379.2020 PMID: 33356944

7. Reijrink M, de Boer SA, Spoor DS, Lefrandt JD, Lambers Heerspink HJ, Boellaard R, et al. Visceral adipose tissue volume is associated with premature atherosclerosis in early type 2 diabetes mellitus independent of traditional risk factors. Atherosclerosis. 2019;290:87–93. https://doi.org/10.1016/j.atherosclerosis.2019.09.016 PMID: 31604171

8. Vallejo J, Cochain C, Zernecke A, Ley K. Heterogeneity of immune cells in human atherosclerosis revealed by scRNA-Seq. Cardiovasc Res. 2021;117(13):2537–43. https://doi.org/10.1093/cvr/cvab260 PMID: 34343272

9. Fernandez DM, Rahman AH, Fernandez NF, Chudnovskiy A, Amir E-AD, Amadori L, et al. Single-cell immune landscape of human atherosclerotic plaques. Nat Med. 2019;25(10):1576–88. https://doi.org/10.1038/s41591-019-0590-4 PMID: 31591603

10. Ouchi N, Parker JL, Lugus JJ, Walsh K. Adipokines in inflammation and metabolic disease. Nat Rev Immunol. 2011;11(2):85–97. https://doi.org/10.1038/nri2921 PMID: 21252989

11. Cai X, Hua S, Deng J, Du Z, Zhang D, Liu Z, et al. Astaxanthin Activated the Nrf2/HO-1 Pathway to enhance autophagy and inhibit ferroptosis, ameliorating acetaminophen-induced liver injury. ACS Appl Mater Interfaces. 2022;14(38):42887–903. https://doi.org/10.1021/acsami.2c10506 PMID: 36094079

12. Li J, Guo C, Wu J. Astaxanthin in liver health and disease: a potential therapeutic agent. Drug Des Devel Ther. 2020;14:2275–85. https://doi.org/10.2147/DDDT.S230749 PMID: 32606597

13. Kohandel Z, Farkhondeh T, Aschner M, Pourbagher-Shahri AM, Samarghandian S. Anti-inflammatory action of astaxanthin and its use in the treatment of various diseases. Biomed Pharmacother. 2022;145:112179. https://doi.org/10.1016/j.biopha.2021.112179 PMID: 34736076

14. Dose J, Matsugo S, Yokokawa H, Koshida Y, Okazaki S, Seidel U, et al. Free radical scavenging and cellular antioxidant properties of astaxanthin. IJMS. 2016 Jan 14;17(1):103.

15. Zaafan MA, Abdelhamid AM. The cardioprotective effect of astaxanthin against isoprenaline-induced myocardial injury in rats: involvement of TLR4/NF-κB signaling pathway. Eur Rev Med Pharmacol Sci. 2021;25(11):4099–105. https://doi.org/10.26355/eurrev_202106_26052 PMID: 34156689

16. Choi HD, Youn YK, Shin WG. Positive effects of astaxanthin on lipid profiles and oxidative stress in overweight subjects. Plant Foods Hum Nutr. 2011;66(4):363–9. https://doi.org/10.1007/s11130-011-0258-9 PMID: 21964877

17. Karppi J, Rissanen TH, Nyyssönen K, Kaikkonen J, Olsson AG, Voutilainen S, et al. Effects of astaxanthin supplementation on lipid peroxidation. Int J Vitam Nutr Res. 2007;77(1):3–11. https://doi.org/10.1024/0300-9831.77.1.3 PMID: 17685090

18. Yoshida H, Yanai H, Ito K, Tomono Y, Koikeda T, Tsukahara H, et al. Administration of natural astaxanthin increases serum HDL-cholesterol and adiponectin in subjects with mild hyperlipidemia. Atherosclerosis. 2010;209(2):520–3. https://doi.org/10.1016/j.atherosclerosis.2009.10.012 PMID: 19892350

19. Arunkumar E, Bhuvaneswari S, Anuradha CV. An intervention study in obese mice with astaxanthin, a marine carotenoid–effects on insulin signaling and pro-inflammatory cytokines. Food Funct. 2012;3(2):120–6. https://doi.org/10.1039/c1fo10161g PMID: 22089895

20. Wakabayashi K, Hamada C, Kanda R, Nakano T, Io H, Horikoshi S. Oral astaxanthin supplementation prevents peritoneal fibrosis in rats. Perit Dial Int. 2015;35(5):506–16.

21. Liu D, Ji Y, Cheng Q, Zhu Y, Zhang H, Guo Y, et al. Dietary astaxanthin-rich extract ameliorates atherosclerosis/retinopathy and restructures gut microbiome in apolipoprotein E-deficient mice fed on a high-fat diet. Food Funct. 2022;13(20):10461–75. https://doi.org/10.1039/d2fo02102a PMID: 36134474

22. Zou T-B, Zhu S-S, Luo F, Li W-Q, Sun X-R, Wu H-F. Effects of astaxanthin on reverse cholesterol transport and atherosclerosis in mice. Biomed Res Int. 2017;2017:4625932. https://doi.org/10.1155/2017/4625932 PMID: 29226138

23. Zirlik A, Maier C, Gerdes N, MacFarlane L, Soosairajah J, Bavendiek U. CD40 Ligand mediates inflammation independently of CD40 by interaction with mac-1. Circulation. 2007;115(12):1571–80.

24. Stachon P, Geis S, Peikert A, Heidenreich A, Michel NA, Ünal F, et al. Extracellular ATP induces vascular inflammation and atherosclerosis via purinergic receptor Y2 in mice. Arterioscler Thromb Vasc Biol. 2016;36(8):1577–86. https://doi.org/10.1161/ATVBAHA.115.307397 PMID: 27339459

25. Yushkevich PA, Piven J, Hazlett HC, Smith RG, Ho S, Gee JC, et al. User-guided 3D active contour segmentation of anatomical structures: significantly improved efficiency and reliability. Neuroimage. 2006;31(3):1116–28. https://doi.org/10.1016/j.neuroimage.2006.01.015 PMID: 16545965

26. Hu HH, Li Y, Nagy TR, Goran MI, Nayak KS. Quantification of absolute fat mass by magnetic resonance imaging: a validation study against chemical analysis. Int J Body Compos Res. 2011;9(3):111–22. PMID: 23204926

27. Bredies K, Kunisch K, Pock T. Total generalized variation. SIAM J Imaging Sci. 2010;3(3):492–526.

28. Anto Michel N, Colberg C, Buscher K, Sommer B, Pramod AB, Ehinger E, et al. Inflammatory pathways regulated by tumor necrosis receptor-associated factor 1 protect from metabolic consequences in diet-induced obesity. Circ Res. 2018;122(5):693–700. https://doi.org/10.1161/CIRCRESAHA.117.312055 PMID: 29358227

29. Horstmann H, Michel NA, Sheng X, Hansen S, Lindau A, Pfeil K, et al. Cross-species single-cell RNA sequencing reveals divergent phenotypes and activation states of adaptive immunity in human carotid and experimental murine atherosclerosis. Cardiovasc Res. 2024;120(14):1713–26. https://doi.org/10.1093/cvr/cvae154 PMID: 39041203

30. Wolf D, Anto-Michel N, Blankenbach H, Wiedemann A, Buscher K, Hohmann JD, et al. A ligand-specific blockade of the integrin Mac-1 selectively targets pathologic inflammation while maintaining protective host-defense. Nat Commun. 2018;9(1):525. https://doi.org/10.1038/s41467-018-02896-8 PMID: 29410422

31. Hansson GK, Libby P, Tabas I. Inflammation and plaque vulnerability. J Intern Med. 2015;278(5):483–93. https://doi.org/10.1111/joim.12406 PMID: 26260307

32. Leipner J, Dederichs T-S, von Ehr A, Rauterberg S, Ehlert C, Merz J, et al. Myeloid cell-specific Irf5 deficiency stabilizes atherosclerotic plaques in Apoe$^{-/-}$ mice. Mol Metab. 2021;53:101250. https://doi.org/10.1016/j.molmet.2021.101250 PMID: 33991749

33. Gissler MC, Scherrer P, Anto-Michel N, Pennig J, Hoppe N, Füner L, et al. Deficiency of endothelial CD40 induces a stable plaque phenotype and limits inflammatory cell recruitment to atherosclerotic lesions in mice. Thromb Haemost. 2021;121(11):1530–40. https://doi.org/10.1055/a-1397-1858 PMID: 33618394

34. Swirski FK, Libby P, Aikawa E, Alcaide P, Luscinskas FW, Weissleder R, et al. Ly-6Chi monocytes dominate hypercholesterolemia-associated monocytosis and give rise to macrophages in atheromata. J Clin Invest. 2007;117(1):195–205. https://doi.org/10.1172/JCI29950 PMID: 17200719

35. Hilgendorf I, Gerhardt LMS, Tan TC, Winter C, Holderried TAW, Chousterman BG. Ly-6Chigh monocytes depend on Nr4a1 to balance both inflammatory and reparative phases in the infarcted myocardium. Circulation Research. 2014;114(10):1611–22.

36. Hartvigsen K, Binder CJ, Hansen LF, Rafia A, Juliano J, Hörkkö S, et al. A diet-induced hypercholesterolemic murine model to study atherogenesis without obesity and metabolic syndrome. Arterioscler Thromb Vasc Biol. 2007;27(4):878–85. https://doi.org/10.1161/01.ATV.0000258790.35810.02 PMID: 17255537

37. Neuhofer A, Wernly B, Leitner L, Sarabi A, Sommer NG, Staffler G, et al. An accelerated mouse model for atherosclerosis and adipose tissue inflammation. Cardiovasc Diabetol. 2014;13:23. https://doi.org/10.1186/1475-2840-13-23 PMID: 24438079

38. Missiou A, Wolf D, Platzer I, Ernst S, Walter C, Rudolf P, et al. CD40L induces inflammation and adipogenesis in adipose cells–a potential link between metabolic and cardiovascular disease. Thromb Haemost. 2010;103(4):788–96. https://doi.org/10.1160/TH09-07-0463 PMID: 20174757

39. Bonfleur ML, Vanzela EC, Ribeiro RA, de Gabriel Dorighello G, de França Carvalho CP, Collares-Buzato CB, et al. Primary hypercholesterolaemia impairs glucose homeostasis and insulin secretion in low-density lipoprotein receptor knockout mice independently of high-fat diet and obesity. Biochim Biophys Acta. 2010;1801(2):183–90. https://doi.org/10.1016/j.bbalip.2009.10.012 PMID: 19913637

40. Bugger H, Zirlik A. Anti-inflammatory strategies in atherosclerosis. Hamostaseologie. 2021;41(6):433–42. https://doi.org/10.1055/a-1661-0020 PMID: 34942656

41. Ridker PM, Everett BM, Thuren T, MacFadyen JG, Chang WH, Ballantyne C. Antiinflammatory therapy with canakinumab for atherosclerotic disease. N Engl J Med. 2017;377(12):1119–31.

42. Ait-Oufella H, Libby P. Inflammation and atherosclerosis: prospects for clinical trials. Arterioscler Thromb Vasc Biol. 2024;44(9):1899–905. https://doi.org/10.1161/ATVBAHA.124.320155 PMID: 39167675

43. Michel NA, Zirlik A, Wolf D. CD40L and its receptors in atherothrombosis-an update. Front Cardiovasc Med. 2017;4:40. https://doi.org/10.3389/fcvm.2017.00040 PMID: 28676852

44. Tardif JC, Kouz S, Waters DD, Bertrand OF, Diaz R, Maggioni AP. Efficacy and safety of low-dose colchicine after myocardial infarction. N Engl J Med. 2019;381(26).

45. Calbi V, Fumagalli F, Consiglieri G, Penati R, Acquati S, Redaelli D, et al. Use of Defibrotide to help prevent post-transplant endothelial injury in a genetically predisposed infant with metachromatic leukodystrophy undergoing hematopoietic stem cell gene therapy. Bone Marrow Transplant. 2018;53(7):913–7. https://doi.org/10.1038/s41409-017-0085-1 PMID: 29379168

46. Zirlik A, Bavendiek U, Libby P, MacFarlane L, Gerdes N, Jagielska J. TRAF-1, -2, -3, -5, and -6 are induced in atherosclerotic plaques and differentially mediate proinflammatory functions of CD40L in endothelial cells. Arterioscler Thromb Vasc Biol. 2007;27(5):1101–7.

47. Willecke F, Rupprecht B, Gissler MC, Pfeiffer K, Anto-Michel N, Stachon P, et al. Tumor necrosis factor receptor-associated factor 5 promotes arterial neointima formation through smooth muscle cell proliferation. J Vasc Res. 2019;56(6):308–19. https://doi.org/10.1159/000501615 PMID: 31437850

48. Gissler MC, Anto-Michel N, Pennig J, Scherrer P, Li X, Marchini T, et al. Genetic deficiency of TRAF5 promotes adipose tissue inflammation and aggravates diet-induced obesity in mice. Arterioscler Thromb Vasc Biol. 2021;41(10):2563–74. https://doi.org/10.1161/ATVBAHA.121.316677 PMID: 34348490

49. Wolf D, Bukosza N, Engel D, Poggi M, Jehle F, Anto Michel N. Inflammation, but not recruitment, of adipose tissue macrophages requires signalling through Mac-1 (CD11b/CD18) in diet-induced obesity (DIO). Thromb Haemost. 2017;117(2):325–38.

50. Chang MX, Xiong F. Astaxanthin and its effects in inflammatory responses and inflammation-associated diseases: recent advances and future directions. Molecules. 2020;25(22):5342. https://doi.org/10.3390/molecules25225342

51. Ryu SK, King TJ, Fujioka K, Pattison J, Pashkow FJ, Tsimikas S. Effect of an oral astaxanthin prodrug (CDX-085) on lipoprotein levels and progression of atherosclerosis in LDLR$^{-/-}$ and ApoE$^{-/-}$ mice. Atherosclerosis. 2012;222(1):99–105. https://doi.org/10.1016/j.atherosclerosis.2012.02.002 PMID: 22406426

52. Eilertsen K-E, Mæhre HK, Jensen IJ, Devold H, Olsen JO, Lie RK, et al. A wax ester and astaxanthin-rich extract from the marine copepod *Calanus finmarchicus* attenuates atherogenesis in female apolipoprotein E-deficient mice. J Nutr. 2012;142(3):508–12. https://doi.org/10.3945/jn.111.145698 PMID: 22323762

53. Zhang Z, Qiu Y, Li W, Tang A, Huang H, Yao W, et al. Astaxanthin alleviates foam cell formation and promotes cholesterol efflux in Ox-LDL-Induced RAW264.7 cells via CircTPP2/miR-3073b-5p/ABCA1 pathway. Molecules. 2023 Feb 10;28(4):1701.

54. Pérez S, Rius-Pérez S. Macrophage polarization and reprogramming in acute inflammation: a redox perspective. Antioxidants (Basel). 2022;11(7):1394. https://doi.org/10.3390/antiox11071394 PMID: 35883885

55. Wu J, He S, Song Z, Chen S, Lin X, Sun H, et al. Macrophage polarization states in atherosclerosis. Front Immunol. 2023;14:1185587. https://doi.org/10.3389/fimmu.2023.1185587 PMID: 37207214

56. Xie Y, Chen H, Qu P, Qiao X, Guo L, Liu L. Novel insight on the role of Macrophages in atherosclerosis: focus on polarization, apoptosis and efferocytosis. Int Immunopharmacol. 2022;113(Pt A):109260. https://doi.org/10.1016/j.intimp.2022.109260 PMID: 36252496

57. Barrett TJ. Macrophages in atherosclerosis regression. Arterioscler Thromb Vasc Biol. 2020;40(1):20–33. https://doi.org/10.1161/ATV-BAHA.119.312802 PMID: 31722535

58. Xie W-J, Hou G, Wang L, Wang S-S, Xiong X-X. Astaxanthin suppresses lipopolysaccharide-induced myocardial injury by regulating MAPK and PI3K/AKT/mTOR/GSK3β signaling. Mol Med Rep. 2020;22(4):3338–46. https://doi.org/10.3892/mmr.2020.11443 PMID: 32945516

59. Chen J-C, Wu C-H, Peng Y-S, Zheng H-Y, Lin Y-C, Ma P-F, et al. Astaxanthin enhances erlotinib-induced cytotoxicity by p38 MAPK mediated xeroderma pigmentosum complementation group C (XPC) down-regulation in human lung cancer cells. Toxicol Res (Camb). 2018;7(6):1247–56. https://doi.org/10.1039/c7tx00292k PMID: 30555679

60. Canault M, Peiretti F, Poggi M, Mueller C, Kopp F, Bonardo B, et al. Progression of atherosclerosis in ApoE-deficient mice that express distinct molecular forms of TNF-alpha. J Pathol. 2008;214(5):574–83. https://doi.org/10.1002/path.2305 PMID: 18247429

61. Garbers C, Hermanns HM, Schaper F, Müller-Newen G, Grötzinger J, Rose-John S, et al. Plasticity and cross-talk of interleukin 6-type cytokines. Cytokine Growth Factor Rev. 2012;23(3):85–97. https://doi.org/10.1016/j.cytogfr.2012.04.001 PMID: 22595692

62. Fatkhullina AR, Peshkova IO, Koltsova EK. The role of cytokines in the development of atherosclerosis. Biochemistry (Mosc). 2016;81(11):1358–70. https://doi.org/10.1134/S0006297916110134 PMID: 27914461

63. Kirii H, Niwa T, Yamada Y, Wada H, Saito K, Iwakura Y, et al. Lack of interleukin-1beta decreases the severity of atherosclerosis in ApoE-deficient mice. Arterioscler Thromb Vasc Biol. 2003;23(4):656–60. https://doi.org/10.1161/01.ATV.0000064374.15232.C3 PMID: 12615675

64. Fontes JA, Rose NR, Čiháková D. The varying faces of IL-6: from cardiac protection to cardiac failure. Cytokine. 2015;74(1):62–8. https://doi.org/10.1016/j.cyto.2014.12.024 PMID: 25649043

65. Sethi JK, Hotamisligil GS. Metabolic messengers: tumour necrosis factor. Nat Metab. 2021;3(10):1302–12.

66. Wellen KE, Hotamisligil GS. Inflammation, stress, and diabetes. J Clin Invest. 2005;115(5):1111–9. https://doi.org/10.1172/JCI25102 PMID: 15864338

67. Al-Roub A, Al Madhoun A, Akhter N, Thomas R, Miranda L, Jacob T, et al. IL-1β and TNFα cooperativity in regulating IL-6 expression in adipocytes depends on CREB binding and H3K14 acetylation. Cells. 2021;10(11):3228. https://doi.org/10.3390/cells10113228 PMID: 34831450

68. Fuster JJ, Ouchi N, Gokce N, Walsh K. Obesity-induced changes in adipose tissue microenvironment and their impact on cardiovascular disease. Circ Res. 2016;118(11):1786–807.

69. Osborn O, Olefsky JM. The cellular and signaling networks linking the immune system and metabolism in disease. Nat Med. 2012;18(3):363–74.

70. da Cruz Nascimento SS, Carvalho de Queiroz JL, Fernandes de Medeiros A, de França Nunes AC, Piuvezam G, Lima Maciel BL, et al. Anti-inflammatory agents as modulators of the inflammation in adipose tissue: a systematic review. PLoS One. 2022;17(9):e0273942. https://doi.org/10.1371/journal.pone.0273942 PMID: 36048868

71. Kawai T, Autieri MV, Scalia R. Adipose tissue inflammation and metabolic dysfunction in obesity. Am J Physiol Cell Physiol. 2021;320(3):C375-91.

72. Omran F, Christian M. Inflammatory signaling and brown fat activity. Front Endocrinol. 2020;11:156.

73. Merz KE, Thurmond DC. Role of skeletal muscle in insulin resistance and glucose uptake. Compr Physiol. 2020;10(3):785–809. https://doi.org/10.1002/cphy.c190029 PMID: 32940941